On the evaluation of mechanical properties of honeycombs by using finite element analyses

Stefan SOROHAN*,[1], Marin SANDU[1], Dan Mihai CONSTANTINESCU[1], Adriana Georgeta SANDU[1]

*Corresponding author
[1]Department of Strength of Materials, "POLITEHNICA" University of Bucharest
Splaiul Independenţei 313, 060042, Bucharest, Romania
stefan.sorohan@upb.ro*, marin.sandu@upb.ro, dan.constantinescu@upb.ro, adriana.sandu@upb.ro

DOI: 10.13111/2066-8201.2015.7.3.13

Received: 22 july 2015 / Accepted: 13 august 2015

Abstract: *This paper presents some general two- and three-dimensional finite element models to study the equivalent orthotropic mechanical properties of honeycombs. The models are developed on a representative volume element with appropriate periodic boundary conditions for six load cases for three-dimensional models to obtain the in-plane and out-of-plane elastic properties of hexagonal honeycombs. The developed models use beam, solid 2D and 3D, and also shell type finite elements. The proposed models are validated using analytical relationships from literature. For this reason some aspects regarding their proper use, depending on the purpose of the analysis, are presented. It is shown that similar models can be used for different periodic cell structures as chiral and anti-chiral honeycomb structures. The developed finite element models can also be used conveniently for parametric and sensitivity analyses because the total number of degrees of freedom is relatively small compared to a complete model.*

Key Words*: Mechanical properties, Honeycombs, Finite elements, Periodic Boundary Conditions, Young's moduli, Poisson's ratios, Representative Volume Element.*

1. INTRODUCTION

Usually the term *honeycomb* is used in a broader sense to describe any array of identical prismatic cells which nest together to fill a plate. The cells are typically hexagonal, in cross-section, but they can also be triangular, square or rhombic. Because honeycombs have a regular geometry their deformations can be analyzed more or less exactly to give equations which describe their mechanical equivalent properties, [1].

In order to simplify the static or dynamic analysis of structures achieved with heterogeneous materials (Fig. 1), it is extremely useful to estimate the homogenized constitutive behaviours of such materials subjected to small and even large deformations. Actually, the analysis of such structures can be divided into two sequential problems [2, 3]. In the first problem (micro-problem) the global behaviour of a so called Representative Volume Element (RVE) is determined. In particular the RVE (Fig. 2) of the microstructure can be a single unit cell member [3-10], or a particular assembly of unity cells [11-15]. From the solution of the micro-problem the global constitutive properties are derived. These

properties are then used in the second problem (macro-problem) in order to analyze the behaviour of the macroscopic structure subjected to given loads.

Usually, in a Finite Element Analysis (FEA), the macroscopic model of a panel, like the one presented in Fig. 1, can be modelled as a layered composite Shell with sandwich option or as a solid structure in which the core is discretized with orthotropic brick elements [4,16].

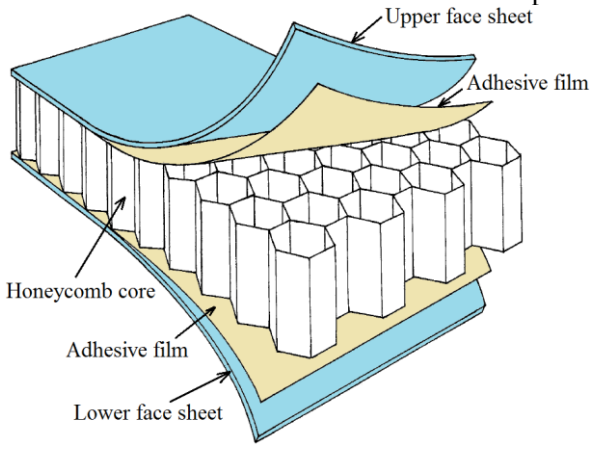

Fig. 1 – Honeycomb panel

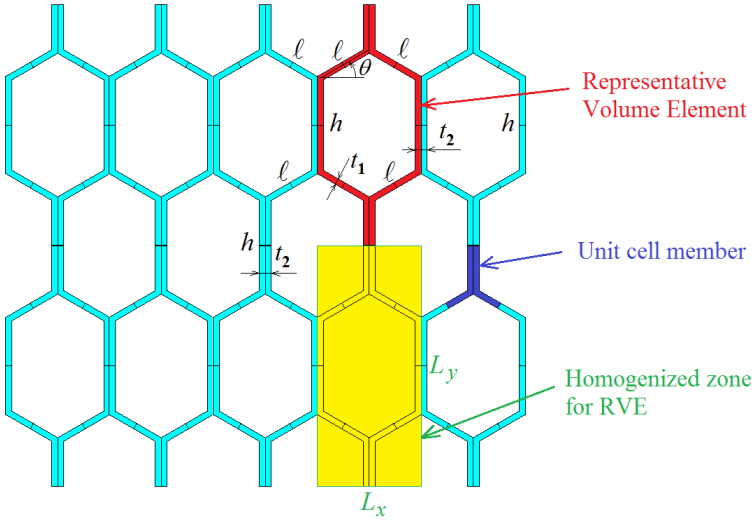

Fig. 2 – Part of the core model - periodic cell, that is sometimes analyzed using FEA to obtain the equivalent elastic properties and RVE considered in this paper

Explicit modeling of the complete core can increase very much the total number of finite elements and of course the number of Degrees Of Freedom (DOFs) which must be solved, increasing the computation effort without real benefits for some practical problems.

In this paper, the same RVE is considered for all developed finite element models. Such an assumption requires the analysis of the RVE composed by an optimal assembly of unit cells. Usually, the RVE is subjected to an enforced displacement path on its boundary [16]. The RVE boundary conditions influence the FEA evaluations [4, 11] and careful choice of the displacements must be considered according to the real deformations for each load case.

Some analytical relations for equivalent mechanical properties estimations [1, 2, 17, 18] are also considered in the literature. Gibson and Ashby [1] summarized the analytical

formulas for relative density and the in-plane and out-of-plane properties of some honeycombs. The considered honeycombs are the *classical* ones, in which the thickness of the all walls is constant, but also for hexagonal honeycombs with double walls attached by gluing along the ribbon direction, which are called sometimes *commercial honeycombs*. All these formulas are obtained principally by using the beam model theory. Currently, analytical models of elements composing honeycombs assemblies are being refined to include axial and shear deformations, in addition to bending deformations, on which all first studies have been based. Such refinements provide an additional insight into the mechanical behaviour of honeycomb assemblies and may suggest additional, unexplored applications.

The resulting fundamental deformation mechanisms associated with such deformations can be determined easier if some finite element models are developed based on a large number of cells from the analyzed structure (see Fig. 2) because, according to the Saint Venant's principle, the approximations in the boundary conditions may lightly affect the response of a cell in the middle of the analyzed model. Such methodologies were used in many papers [11, 12-14], and even if not presented, they were also developed and used in the present paper for verification purposes. In this way it was confirmed that the displacements, reactions, strain energy and also stresses in RVE analysis were identical to those observed in numerical studies involving a full similar lattice with more than ten cells multiplied on each direction. The parametric conceptual model developed and analyzed in this paper is presented in Fig. 3. It may represent classical and commercial honeycombs, but also re-entrant honeycombs if $\theta < 0$.

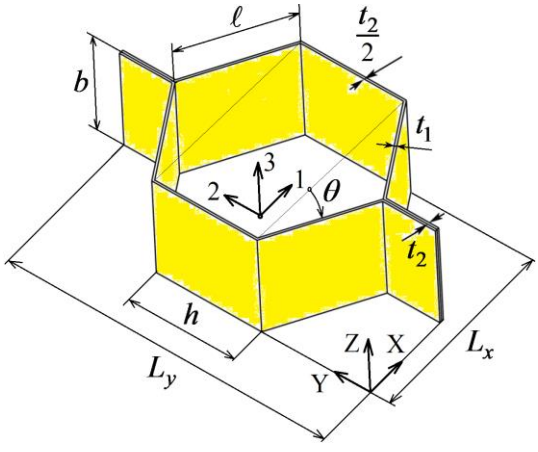

Fig. 3 – Notation of geometrical parameters of RVE

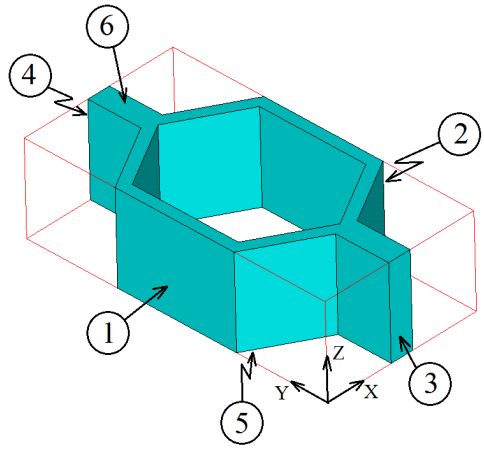

Fig. 4 – Faces notation of RVE

2. ANALYTICAL BACKGROUND

Using the beam theory [1, 2] the equivalent mechanical properties of honeycombs can be obtained starting with isotropic constants of the core material: ρ_s - mass density, E_s - Young's modulus and ν_s - Poisson's ratio. The shear modulus is obtained from $G_s = E_s / \left[2(1+\nu_s)\right]$.

For an equivalent *orthotropic material*, with the principal directions along the axes of the system OXYZ (Fig. 3), according to the generalized Hooke's law, it yields $\bar{\boldsymbol{\varepsilon}} = \boldsymbol{C}\bar{\boldsymbol{\sigma}}$, where $\bar{\boldsymbol{\varepsilon}}$ and $\bar{\boldsymbol{\sigma}}$ are the strain and respectively the stress vector of the homogenized region of the RVE. The compliance matrix, which includes the equivalent mechanical elastic properties, is [16, 19]

$$\boldsymbol{C}=\begin{bmatrix} \frac{1}{E_1} & -\frac{\nu_{12}}{E_2} & -\frac{\nu_{13}}{E_3} & 0 & 0 & 0 \\ -\frac{\nu_{21}}{E_1} & \frac{1}{E_2} & -\frac{\nu_{23}}{E_3} & 0 & 0 & 0 \\ -\frac{\nu_{31}}{E_1} & -\frac{\nu_{32}}{E_2} & \frac{1}{E_3} & 0 & 0 & 0 \\ 0 & 0 & 0 & \frac{1}{G_{12}} & 0 & 0 \\ 0 & 0 & 0 & 0 & \frac{1}{G_{23}} & 0 \\ 0 & 0 & 0 & 0 & 0 & \frac{1}{G_{13}} \end{bmatrix}. \tag{1}$$

Owing to the symmetry, the following equations must exist:

$$\frac{\nu_{21}}{E_1}=\frac{\nu_{12}}{E_2};\quad \frac{\nu_{31}}{E_1}=\frac{\nu_{13}}{E_3};\quad \frac{\nu_{32}}{E_2}=\frac{\nu_{23}}{E_3}. \tag{2}$$

First, we present the derived relationships for classical honeycombs, i.e. for $t_1=t_2=t$ (Fig. 3) and then, for commercial honeycombs, i.e. for $t_1=t$ and $t_2=2t$ [1, 20, 21].

2.1 Classical honeycombs. The relative density of the equivalent core is

$$\frac{\rho}{\rho_s}=\frac{\frac{t}{\ell}\left(\frac{h}{\ell}+2\right)}{2\left(\frac{h}{\ell}+\sin\theta\right)\cos\theta}. \tag{3}$$

2.1.1 In plane elastic properties. The Young's moduli parallel to OX and OY are

$$E_1=k_1E_s\left(\frac{t}{\ell}\right)^3\frac{\cos\theta}{\left(\frac{h}{\ell}+\sin\theta\right)\sin^2\theta};\quad E_2=k_2E_s\left(\frac{t}{\ell}\right)^3\frac{\frac{h}{\ell}+\sin\theta}{\cos^3\theta} \tag{4}$$

where

$$k_1=\frac{1}{1+\left(\frac{t}{\ell}\right)^2\left(2.4+1.5\nu_s+\cot^2\theta\right)};\ k_2=\frac{1}{1+\left(\frac{t}{\ell}\right)^2\left(2.4+1.5\nu_s+\tan^2\theta+2\frac{h}{\ell\cos^2\theta}\right)}. \tag{5}$$

The in plane Poisson's ratios can be calculated using

$$\nu_{12}=c_{12}\frac{\cos^2\theta}{\left(\frac{h}{\ell}+\sin\theta\right)\sin\theta};\quad \nu_{21}=c_{21}\frac{\left(\frac{h}{\ell}+\sin\theta\right)\sin\theta}{\cos^2\theta}, \tag{6}$$

where

$$c_{12}=\frac{1+\left(\frac{t}{\ell}\right)^2\left(1.4+1.5\nu_s\right)}{1+\left(\frac{t}{\ell}\right)^2\left(2.4+1.5\nu_s+\cot^2\theta\right)};\ c_{21}=\frac{1+\left(\frac{t}{\ell}\right)^2\left(1.4+1.5\nu_s\right)}{1+\left(\frac{t}{\ell}\right)^2\left(2.4+1.5\nu_s+\tan^2\theta+2\frac{h}{\ell\cos^2\theta}\right)}. \quad (7)$$

The in plane shear modulus is

$$G_{12}=k_{12}E_s\left(\frac{t}{\ell}\right)^3\frac{\frac{h}{\ell}+\sin\theta}{\left(\frac{h}{\ell}\right)^2\left(1+\frac{2h}{\ell}\right)\cos\theta}, \quad (8)$$

where

$$k_{12}=\frac{\left(1+\frac{2h}{\ell}\right)}{1+\frac{2h}{\ell}+\left(\frac{t}{\ell}\right)^2\left\{\frac{\ell}{h}\left(2.4+1.5\nu_s\right)\left(2+\frac{h}{\ell}+\sin\theta\right)+\frac{\frac{h}{\ell}+\sin\theta}{\left(\frac{h}{\ell}\right)^2}\left[\left(\frac{h}{\ell}+\sin\theta\right)\tan^2\theta+\sin\theta\right]\right\}} \quad (9)$$

The coefficients, or correction factors, k_1, k_2, k_{12}, c_{12} and c_{21} become equal to 1 if the axial and shearing force contributions to the total strain energy are neglected.

2.1.2 Out of plane elastic properties. The Young's modulus parallel to OZ, and Poisson's ratios due to a load along OZ axis are simply set to

$$E_3=E_s\frac{\rho}{\rho_s};\qquad \nu_{31}=\nu_{32}=\nu_s, \quad (10)$$

and then, according to the reciprocal relations, it results the remainder of Poisson's ratios

$$\nu_{13}=\nu_s\frac{E_1}{E_3};\qquad \nu_{23}=\nu_s\frac{E_2}{E_3}. \quad (11)$$

The following relationships, obtained also in the beam theory hypotheses, are valid only for $t<<\ell$, and $b>>\ell$ because of supplementary hypotheses as the shear stresses are uniform within the cell walls. The two out of plane shear moduli can be obtained from

$$G_{13}=G_s\left(\frac{t}{\ell}\right)\frac{\cos\theta}{\left(\frac{h}{\ell}+\sin\theta\right)};\ G_{23}=G_{23}^L+\frac{\alpha}{\left(\frac{b}{\ell}\right)}\left(G_{23}^U-G_{23}^L\right). \quad (12)$$

The last relation in (12) was deduced by Grediac [20] using the method proposed by Kelsey [21] and FEA in some particular hypothesis (t/ℓ = 0.08, h/ℓ = 1 and $0<\theta<30°$) for which α = 0.787. The upper and lower bounds of shear moduli are obtained from

$$G_{23}^U=\frac{1}{2}G_s\left(\frac{t}{\ell}\right)\frac{\frac{h}{\ell}+2\sin^2\theta}{\left(\frac{h}{\ell}+\sin\theta\right)\cos\theta};\quad G_{23}^L=G_s\left(\frac{t}{\ell}\right)\frac{\frac{h}{\ell}+\sin\theta}{\left(\frac{2h}{\ell}+1\right)\cos\theta}. \quad (13)$$

2.2 Commercial honeycombs. Some relationships obtained for classical honeycombs are also valid for commercial honeycombs [1], so only the modified relations are further presented. The relative density is described by

$$\frac{\rho}{\rho_s}=\frac{\frac{t}{\ell}\left(\frac{h}{\ell}+1\right)}{\left(\frac{h}{\ell}+\sin\theta\right)\cos\theta}. \tag{14}$$

The in plane shear modulus (without correction for axial and shearing forces [1]), was demonstrated by the authors of this paper and its corrected form is

$$G_{12}=E_s\left(\frac{t}{\ell}\right)^3\frac{\frac{h}{\ell}+\sin\theta}{\left(\frac{h}{\ell}\right)^2\left(1+\frac{h}{4\ell}\right)\cos\theta}. \tag{15}$$

The out of plane G_{23} modulus can be also obtained from the second part of Eq. (12), with the same α = 0.787 according to [1], in which the lower and upper bounds of shear modulus are obtained from

$$G_s\left(\frac{t}{\ell}\right)\frac{\frac{h}{\ell}+\sin\theta}{\left(\frac{h}{\ell}+1\right)\cos\theta}\le G_{23}\le G_s\left(\frac{t}{\ell}\right)\frac{\frac{h}{\ell}+\sin^2\theta}{\left(\frac{h}{\ell}+\sin\theta\right)\cos\theta}. \tag{16}$$

3. FINITE ELEMENT HOMOGENIZATION

The aim of the homogenization techniques is to evaluate the global behaviour of a heterogeneous material by studying the response of its RVE, which contains all the geometric and constitutive information of the microstructure. The homogenization consists of replacing the honeycomb structure by an equivalent homogenized orthotropic solid. In fact, the energetic homogenization method is used to determine the elastic properties of the solid [22], but slightly different methods are presented in the literature [3, 7, 16]. The RVE shown in Fig. 2 is used to calculate the equivalent homogenized medium compliance matrix $\boldsymbol{C}$. The homogenization approach is typical for periodic structures that are modelled using finite elements [23]. In a periodic medium, the generalized displacement $\boldsymbol{u}$ can be expressed as $\boldsymbol{u}=\bar{\boldsymbol{\varepsilon}}\boldsymbol{x}+\boldsymbol{u_0}$,where $\bar{\boldsymbol{\varepsilon}}$ is an applied constant strain field, and $\boldsymbol{u_0}$ is a slowly fluctuating periodic function of $\boldsymbol{u}$. This condition is used in the proposed finite element models by means of the couplings between adequate offset of the DOFs on the boundaries [5, 24].

The macroscopic or mean stress and strain vectors $\bar{\boldsymbol{\sigma}}$ and $\bar{\boldsymbol{\varepsilon}}$ are defined by the spatial averages of the stresses and strains in RVE, i.e. [23]

$$\bar{\boldsymbol{\sigma}}=\frac{1}{V}\int_V\boldsymbol{\sigma}dV\,;\qquad \bar{\boldsymbol{\varepsilon}}=\frac{1}{V}\int_V\boldsymbol{\varepsilon}dV\,. \tag{17}$$

Because the stresses and strains are numerically obtained only in some points (Gauss points) and the used commercial finite element code ANSYS does not permit a direct and accurate calculation of the integrals in (17), instead of volume stress averaging (which equivalently can also be transformed into area stress averaging on boundaries), the more

exact method, by dividing the sum of the reaction force to proper cross section area of the homogenized zone is used. Also the macroscopic strain is obtained directly from the displacements of the boundaries, by simple algebra [14, 22, 24].

In computations of materials characterized by a periodic structure and subjected to some load cases, the RVE may be made by an adequate number of unit cells. In this paper the RVE is presented in Figs. 2 - 4 and was thus chosen because the boundary conditions are easier to be identified directly in DOFs defined in the Cartesian global system of coordinates.

The periodic boundary conditions, for each load case, considered in turn to obtain only one nonzero mean stress component, are developed and checked by authors, and are presented in Table 1. Because there are six stress components in the mean stress vector, there were considered six different load cases [22]. It must be noted that faces 5 and 6 are leaved uncoupled and, for example, the displacements and rotations difference of disguised DOFs are defined according to the relations of this form: $u_{xDiff}\,|_{1-2} = u_x(L_x, y, z) - u_x(0, y, z)$, for displacements from faces 1 and 2 along OX direction and $\varphi_{xDiff}\,|_{3-4} = \varphi_x(x, L_y, z) - \varphi_x(x, 0, z)$ for rotations from faces 3 and 4 around the same OX axis. If a model does not include rotational DOFs, the periodic boundary conditions from columns six to eight in Table 1 must be neglected. The same rules are applied also for supplementary DOFs of two dimensional models.

Table 1 – Periodic boundary conditions applied to pair faces of the RVE

Load Case	Pair faces	u_{xDiff}	u_{yDiff}	u_{zDiff}	φ_{xDiff}	φ_{yDiff}	φ_{zDiff}
1	1-2	-	0	0	0	0	0
Axial X	3-4	0	-	0	0	0	0
2	1-2	-	0	0	0	0	0
Axial Y	3-4	0	-	0	0	0	0
3	1-2	-	0	0	0	0	0
Axial Z	3-4	0	-	0	0	0	0
4	1-2	0	0	0	0	0	0
Shear XY	3-4	-	0	0	0	0	0
5	1-2	0	0	0	0	0	0
Shear YZ	3-4	0	0	0	0	0	0
6	1-2	0	0	0	0	0	0
Shear XZ	3-4	0	0	0	0	0	0

In the presented finite element models, for each load case, the conditions that only one component of mean stress is nonzero are guaranteed if the supplementary boundary conditions from Table 2 are fulfilled. In this table u_x, u_y and u_z are displacement DOFs and φ_x, φ_y and φ_z are rotation DOFs.

"Coupled" means that all DOFs in a face are enforced to be equal, due to the symmetry of a load case. "Free" means that the DOFs are leaved free for motion. "B1" means that only one arbitrary DOF on corresponding face and direction, usually, if possible, from a plane of symmetry, is blocked to remove rigid body motion.

The symbol "-" means that the DOFs are already in relations from Table 1 and no more conditions are necessary. The imposed non-zero displacements, as for example $\bar{\varepsilon}_0 L_x$, correspond to an arbitrary user choice of strain $\bar{\varepsilon}_0$, imposed on a direction to ensure the desired symmetry deformations.

It is noted that for all load cases, when possible, the relations (2) and the conditions that only one mean stress component is non-zero, are numerically checked. Moreover, supplementary non-uniform displacements of the deformed free faces are averaged to improve the mean strain deformations used for Poisson's ratios calculation according to their definition [22].

Table 2 – Supplementary displacement boundary conditions for the six load cases used in simulations

Load Case	Face	u_x	u_y	u_z	φ_x	φ_y	φ_z
1 Axial X	1	0	B1	B1	-	-	-
	2	$\bar{\varepsilon}_0 L_x$	-	-	-	-	-
	3	-	Coupled	-	-	-	-
	4	-	Coupled	-	-	-	-
	5	Free	Free	Free	Free	Free	Free
	6	Free	Free	Free	Free	Free	Free
2 Axial Y	1	Coupled	-	-	-	-	-
	2	Coupled	-	-	-	-	-
	3	B1	0	B1	-	-	-
	4	-	$\bar{\varepsilon}_0 L_y$	-	-	-	-
	5	Free	Free	Free	Free	Free	Free
	6	Free	Free	Free	Free	Free	Free
3 Axial Z	1	Coupled	Coupled	Coupled	Coupled	Coupled	Coupled
	2	Coupled	Coupled	Coupled	Coupled	Coupled	Coupled
	3	Coupled	Coupled	Coupled	Coupled	Coupled	Coupled
	4	Coupled	Coupled	Coupled	Coupled	Coupled	Coupled
	5	B1	B1	0	Free	Free	Free
	6	-	-	$\bar{\varepsilon}_0 b$	Free	Free	Free
4 Shear XY	1	-	-	-	-	-	-
	2	-	-	-	-	-	-
	3	0	B1	B1	-	-	-
	4	$\bar{\gamma}_0 L_y$	-	-	-	-	-
	5	Free	Free	Free	Free	Free	Free
	6	Free	Free	Free	Free	Free	Free
5 Shear YZ	1	-	-	-	-	-	-
	2	-	-	-	-	-	-
	3	B1	-	B1	-	-	-
	4	-	-	-	-	-	-
	5	Free	0	Free	Free	Free	Free
	6	Free	$\bar{\gamma}_0 b$	Free	Free	Free	Free
6 Shear XZ	1	-	-	-	-	-	-
	2	-	-	-	-	-	-
	3	-	B1	B1	-	-	-
	4	-	-	-	-	-	-
	5	0	Free	Free	Free	Free	Free
	6	$\bar{\gamma}_0 b$	Free	Free	Free	Free	Free

4. DEVELOPED FINITE ELEMENT MODELS

In this paper we analyze the in plane, and if possible, the out of plane deformations of honeycombs using FEAs with more than a single finite element model. In order to study the equivalent mechanical properties of honeycombs, four different parametric finite element models were developed in ANSYS, using Ansys Programming Design Language (APDL).

The first model is a simple 2D model which can be used in plane stress or plane strain conditions and can use plane quadrilateral linear or quadratic displacement finite elements with only two DOFs per node (Plane182 or Plane183).

The second one is a simple 3D beam model which can use also linear or quadratic elements with seven DOFs per node, three translations, three rotations and warping as a supplementary DOF (Beam188 or Beam189). In this paper the warping effect was neglected.

The third, is a model developed only with Shell elements; it can use linear elements, with four nodes or quadratic one, with eight nodes. Each node has six DOFs, three translations and three rotations, even the normal rotation is approximately introduced (Shell181 or Shell281).

The last finite element model is a 3D solid model which can use linear - eight nodes, or quadratic - 20 nodes, of brick element types (Solid185 or Solid186). The 3D solid finite elements have only three translations per node as DOFs.

It must be pointed out that each model includes the behaviour characteristics of the main hypotheses in which the finite element type was developed. The most accurate and complete models are Shell and Solid 3D models because these models can capture all the nine independent constants from (1). Depending of the aim of the analysis, the model with beams or Solid 2D can also successfully be used in practice usually only for in plane properties of honeycombs or similar chiral or anti-chiral structures [6, 14, 15].

5. MODELS VALIDATION

Case 1: Commercial honeycomb type. In order to validate the proposed models, first an aluminium alloy commercial honeycomb type is considered. The dimensions are: t = 0.1 mm; ℓ =10 mm; h =15 mm; b = 100 mm and θ = 30º and material properties: E_s = 70000 MPa; ν_s = 0.33 and ρ_s = 2700 kg/m^3. For this very thin honeycomb the correction factors in the analytical calculation may be considered to be one.

In order to establish a proper level of discretization of the RVE, a convergence study is carried out. Similar to other works [16, 25] it was found that around of eight linear finite element types per length ℓ, h and b are enough to obtain correct results, but if there are large difference between these dimensions, a good rule of thumb is to consider uniform mesh with mean length of the elements min{ℓ, b, h}/8 for shells and t/2 for solid elements in the thickness direction. If the finite element is quadratic the element size may be two times larger. In this case the element types for all models were quadratic and the total number of elements was 4000 for 2D models, 86 for the beam model, 8600 for the shell model and 22848 for the solid 3D model. The obtained results for this honeycomb are presented in Table 3, for all proposed finite element models. "NA" in this table means not applicable.

It can be observed that almost all FEA results are very close to the analytical ones but there are small discrepancies for some results due to aspects discussed also in the following examples of analysis, where these discrepancies are more accentuated.

Case 2: classical regular honeycomb. The second test case is for a classical regular honeycomb with the following dimensions: $t_1 = t_2 = t$ = 1 mm; $\ell = h$ = 10 mm; b = 15 mm

and θ = 30º and material properties: E_s = 1000 MPa; v_s = 0.3 and ρ_s = 1000 kg/m^3. The thickness of the cells is no more very thin and the analytical relations used for mechanical properties calculation include also the correction coefficients. The mesh of the cross section for all different models is presented in Fig. 5, and the results for quadratic element types are shown in Table 4.

Table 3 – Results for validation of developed models for Case 1

Mechanical property	Analytical	Finite element results				
		2D Models		3D Models		
		Plane stress	Plane strain	Beam	Shell	Solid
ρ [kg/m^3]	38.971	38.881	38.881	38.971	38.971	38.881
E_1 [MPa]	0.12124	0.12379	0.13892	0.12117	0.13573	0.14369
E_2 [MPa]	0.21554	0.22015	0.24707	0.21543	0.24132	0.25555
E_3 [MPa]	1010.4	NA	NA	NA	1010.4	1008.0
G_{12} [MPa]	0.052253	0.053280	0.059793	0.052226	0.058485	0.061371
G_{23} [MPa]	244.89	NA	NA	202.35	238.75	240.01
G_{13} [MPa]	113.95	NA	NA	94.673	101.16	104.71
v_{12}	0.75000	0.74959	0.74959	0.7497	0.74967	0.74953
v_{21}	1.3333	1.3331	1.3331	1.3329	1.3328	1.3330
v_{23}	7.04e-05	NA	NA	NA	7.77e-05	8.39e-05
v_{32}	0.33	NA	NA	NA	0.33	0.33
v_{13}	3.96e-05	NA	NA	NA	4.58e-05	4.68e-05
v_{31}	0.33	NA	NA	NA	0.33	0.33

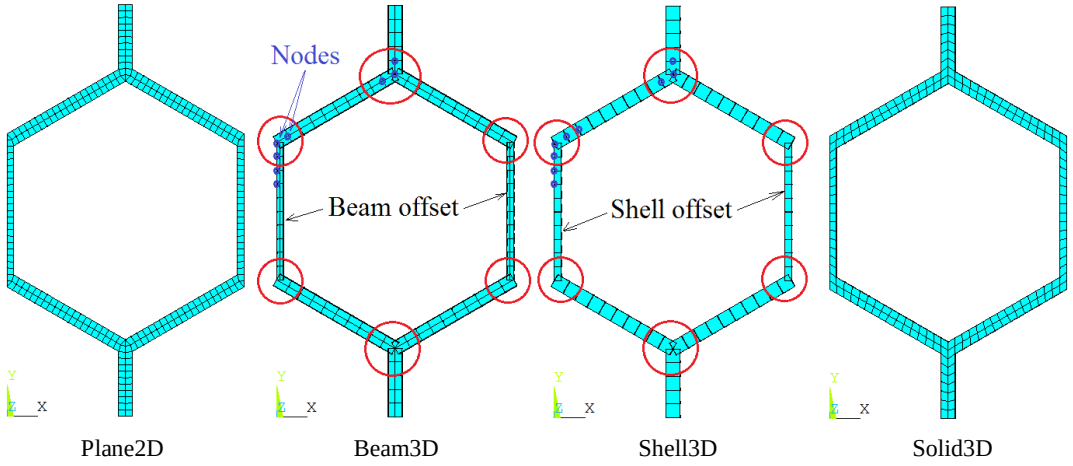

Fig. 5 – Discretization of RVE used for results given in Table 4 (only the cross-sections are shown)

The relative density obtained from accurate FEA (solid models) is almost 3% smaller than the relative density obtained from approximated beam model due to the geometric overlaps at the connection nodes (see marked circles in Fig. 5). Because the hexagon cell is regular and the cell walls are all the same thickness, according to [1] the in plane properties are isotropic (they do not depend on direction): $E = E_1 = E_2$; $v = v_{12} = v_{21}$ and $G_{12}=E/2/(1+v)$. It can be observed that such relations are obtained also from FEA. The out of plane shear moduli obtained from FEA are no more equal and do not respect the relations (12) which are

also approximate or valid for different geometric aspect ratios. It must be mentioned that the vertical beams and shells on laterals (Fig. 5) must be of half thickness and offset to placed nodes exactly on the boundaries of RVE. All the Poisson's ratios are accurately computed using FEA and their values correspond to the analytical ones.

Table 4 – Results for validation of developed models for Case 2

Mechanical property	Analytical	Finite element results				
		2D Models		3D Models		
		Plane stress	Plane strain	Beam	Shell	Solid
ρ [kg/m^3]	115.47	112.14	112.14	115.47	115.47	112.14
E_1 [MPa]	2.1818	2.3491	2.583	2.1767	2.3395	2.583
E_2 [MPa]	2.1818	2.3487	2.5825	2.1767	2.3395	2.5791
E_3 [MPa]	115.47	NA	NA	NA	115.47	112.14
G_{12} [MPa]	0.55610	0.59951	0.65924	0.55463	0.59698	0.65107
G_{23} [MPa]	22.2058	NA	NA	17.670	19.936	20.603
G_{13} [MPa]	22.2058	NA	NA	16.238	15.256	16.793
ν_{12}	0.9622	0.9609	0.96118	0.9623	0.95948	0.95774
ν_{21}	0.9622	0.96074	0.96102	0.9623	0.95948	0.95632
ν_{23}	0.0060	NA	NA	NA	0.006084	0.006835
ν_{32}	0.3000	NA	NA	NA	0.3000	0.3000
ν_{13}	0.0060	NA	NA	NA	0.006073	0.006976
ν_{31}	0.3000	NA	NA	NA	0.3000	0.3000

Case 3: re-entrant classical honeycomb. The third test case is for a re-entrant classical honeycomb with dimensions: $t_1 = t_2 = t = 1$ mm; $\ell = 10$ mm; $h = 30$ mm; $b = 15$ mm and negative internal angle $\theta = -30^o$. Material properties are: $E_s = 1000$ MPa; $\nu_s = 0.3$ and $\rho_s = 1000$ kg/m^3. The analytical relations used for mechanical properties calculation include also the correction coefficients. The mesh of the cross section for all different models is presented in Fig. 6, and the results for quadratic element types are shown in Table 5.

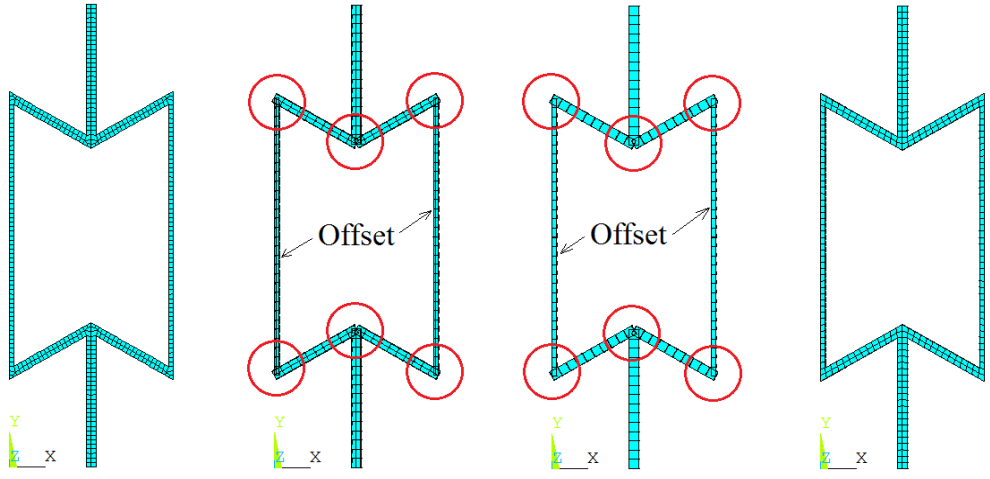

Fig. 6 – Discretization of RVE used for results given in Table 5 (only the cross-sections are shown)

Again the relative density obtained from accurate FEA (solid models) is almost 3% smaller than the relative density obtained from approximated beam model due to the geometric overlaps or gaps at the connection nodes (Fig. 6).

The best FEA corresponds to the solid 3D model, so the comparison of the analytical results is done with this model. Because the hexagon cell is re-entrant, the behaviour of the honeycombs corresponds to an auxetic structure and the in plane Poison's ratios v_{12} and v_{21} are negative and correctly obtained using FEA. The Young's modulus E_1, obtained from FEA is 48% larger than the analytical one, E_2 is 40% larger than the analytical one and G_{12} is 23% larger than the analytical one. These discrepancies are the most probably obtained due to the smaller stiffness in the analytical beam model in the connection points and the effect of small value of *b* parameter which were also reported in the paper of Chen and Ozaki [24], but for regular honeycombs. The out of plane shear moduli G_{23} and G_{13} obtained from FEA are 32% and 22%, respectively, smaller than the analytical ones which also are approximate or valid for different geometric aspect ratios. All the Poisson's ratios are accurately computed using FEAs and their values are close to the analytical ones.

Table 5 – Results for validation of developed models for Case 3

Mechanical property	Analytical	Finite element results				
		2D Models		3D Models		
		Plane stress	Plane strain	Beam	Shell	Solid
ρ [kg/m^3]	115.47	112.14	112.14	115.47	115.47	112.14
E_1 [MPa]	1.3091	1.7663	1.9409	1.3060	1.4044	1.9365
E_2 [MPa]	3.4619	4.4433	4.8827	3.4542	3.6998	4.837
E_3 [MPa]	115.47	NA	NA	NA	115.47	112.14
G_{12} [MPa]	0.04554	0.052029	0.057178	0.045484	0.048399	0.055979
G_{23} [MPa]	23.85	NA	NA	12.956	15.127	16.131
G_{13} [MPa]	13.323	NA	NA	9.7429	8.5635	10.422
v_{12}	-0.57733	-0.58176	-0.58152	-0.57738	-0.57654	-0.58031
v_{21}	-1.5268	-1.4635	-1.4629	-1.5271	-1.5189	-1.4495
v_{23}	0.0100	NA	NA	NA	0.00941	0.01291
v_{32}	0.3000	NA	NA	NA	0.3000	0.3000
v_{13}	0.0036	NA	NA	NA	0.00356	0.00517
v_{31}	0.3000	NA	NA	NA	0.3000	0.3000

6. NUMERICAL SIMULATIONS

6.1 Effect of internal cell angle θ variation. For this study we considered a honeycomb with constant dimensions: $t_1 = t_2 = t = 1$ mm; $\ell = 10$ mm; $h = 20$ mm; $b = 10$ mm and only θ (internal cell angle) was varied between -45º and 45º. The material properties of the cell walls were chosen as before: $E_s = 1000$ MPa; $v_s = 0.3$ and $\rho_s = 1000$ kg/m^3. Using the analytical relations (3) - (13), and the solid 3D finite element model for RVE, the obtained results are presented in Figs. 7 – 10.

From Fig. 7, it can be observed that the equivalent density of the honeycombs has a minimum for θ around 21.5º and the analytical estimations are a little bit larger that the FEA results due to the overlaps (see Fig. 5 and Fig. 6) obtained using beam theory for mass density estimations. This variation in the density is responsible for the same perturbation in

the analytical results as it can be observed very clear for E_3 in Fig. 8, where the FEA results are smaller than the analytical results (more accentuated for negative θ values).

The FEA results for in-plane Young's moduli E_1 and E_2 (Fig. 8) are larger than the analytical results because the cell height b is relatively small (see the results and explanations for the next simulation), but they keep the same variation as the analytical results. The errors decrease with cell angle θ increasing. The same observations are also valid for in-plane shear modulus G_{12} (Fig. 9).

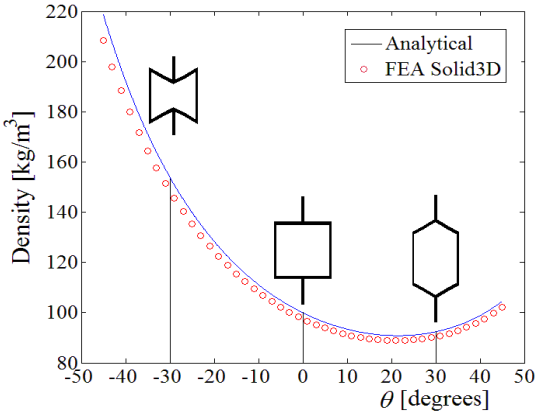

Fig. 7 – Equivalent mass density of the analyzed honeycombs function of internal cell angle

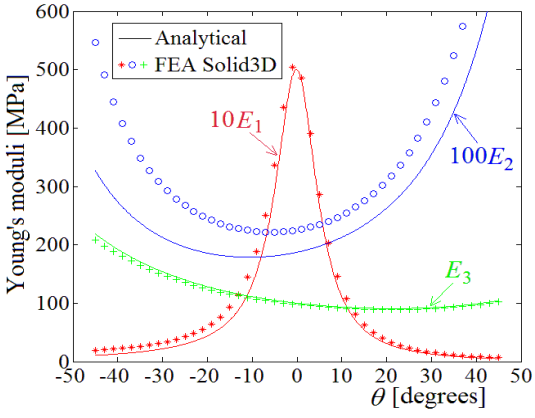

Fig. 8 – Young's moduli of the analyzed honeycombs function of internal cell angle

The FEA results for the out of plane shear modulus G_{13} (Fig. 9) are in excellent agreement (for the considered parameters) with the analytical results only for θ around to zero degrees. Generally, G_{13} is smaller than the analytical result because the cell height b is small and the faces 5 and 6 of the RVE (see Fig. 4) are considered free. The FEA shear modulus G_{23} is relatively close to the analytical result only for $\theta > 0$ (Fig. 9), because the analytical relation (12) is valid only for some particular ratios of geometric parameters - not valid in this case, and positive internal cell angle θ. The upper and lower bounds of G_{23} are plotted with dashed lines and large difference between them appears for large negative internal cell angles. The FEA results of G_{23} for $\theta < 0$ and these particular geometries are more close to the lower bound of G_{23}.

The FEA results for all Poisson's ratios (ν_{31} and ν_{32} which are both 0.3 and are not plotted) are in good agreement with the analytical results (Fig. 10). The largest errors are for very small values of ν_{23} which is very sensitive to E_2 (not very close to the analytical result in this case), according to Eq. (11).

6.2 Effect of cell height *b* variation. This study was developed for the same data as in paragraph 6.1, but for $\theta = 30^\circ$ and the cell height b was varied between 2 mm and 100 mm. The FEA results with significant variation, compared to the analytical ones, are presented in Fig. 11 and Fig. 12, for a finite element model of RVE meshed with four node Shell elements.

All the in plane moduli obtained by using FEA for $\theta = 30^\circ$ (Fig. 11) have a tendency to be around 10% larger than the analytical results when b tends to infinite (plane strain condition). This aspect was also reported in [24] but only for E_2 and was concluded that this effect occurs due to the cells wall deformation in the height direction as ν_s is nonzero. Based on this observation it is now possible to explain the different FEA results compared to the

analytical one for in plane modulus reported in Tables 3-5 and in the previous simulation. It was checked, using FEA, that for $\nu_s = 0$ the effect of increasing the plane moduli disappears.

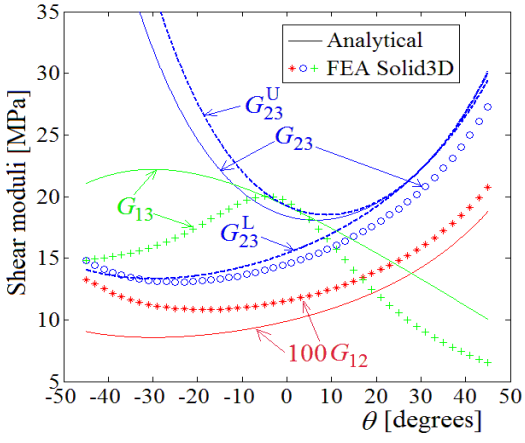

Fig. 9 – Shear moduli of the analyzed honeycombs as functions of internal cell angle

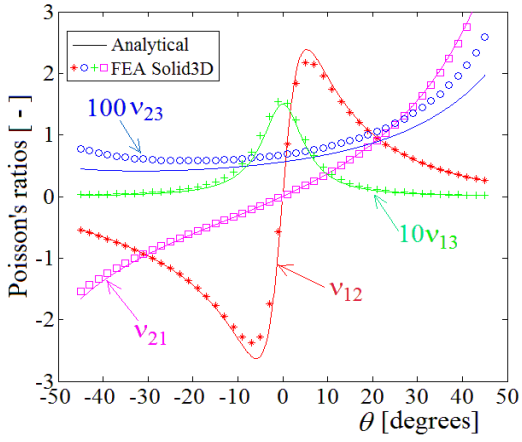

Fig. 10 – Poisson's ratios of the analyzed honeycombs as functions of internal cell angle

Also for the analysed configuration $G_{23}^L = G_{23}^U = G_{23}$, it was observed (Fig. 12) that G_{23} shear modulus obtained with FEA tends to the analytical result if b tends to infinite. For small values of b this shear modulus gives large errors by using the analytical relation which is developed in the hypothesis that almost all the elastic strain energy is stored in the shear displacements of the cell walls, as the bending stiffnesses and the energies associated with bending are much smaller [1]. This hypothesis is not true for small cell height as it can be observed in Fig. 13, where the von Mises stress distribution is presented for four different cell heights in the same loading condition, load case 5 with $\bar{\gamma}_0 =$ 0.026 rad, which corresponds to a maximum shear stress of 10 MPa (around 17.3 MPa von Mises maximum stress). It can be observed that the deformation for a small cell height (b = 5 mm) is different from deformation at an elevated cell height (b = 50 mm) and also the stresses become more uniform and closer to the imposed displacement condition.

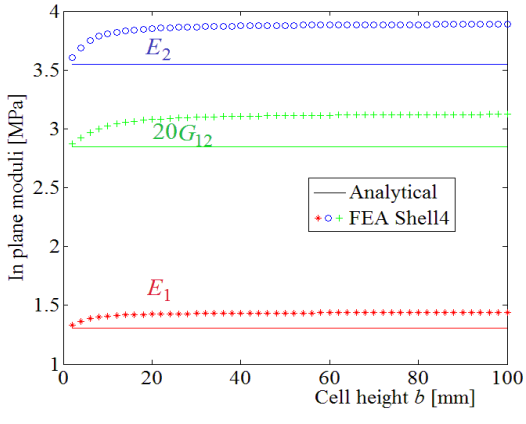

Fig. 11 – The in plane moduli function of cell height variation

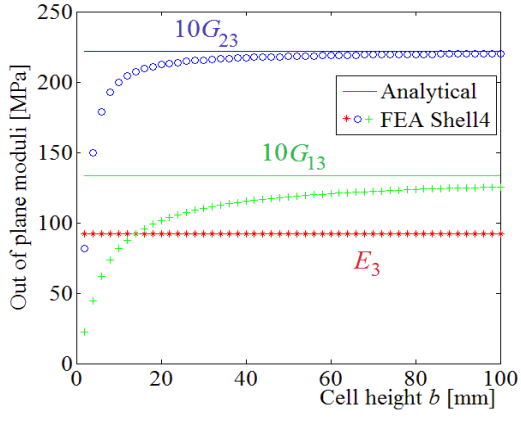

Fig. 12 – The out of plane moduli function of cell height variation

For the analyzed configuration, the shear modulus G_{13} have the same, but with a slower tendency on-coming to the analytical result when b tends to infinite because of the same

previous hypothesis used in the analytical formulation of G_{13}. The out of plane Young's modulus E_3 is independent of b in the FEA results and practically coincides with the analytical result. No important variations of Poisson's ratios were observed in the FEA results.

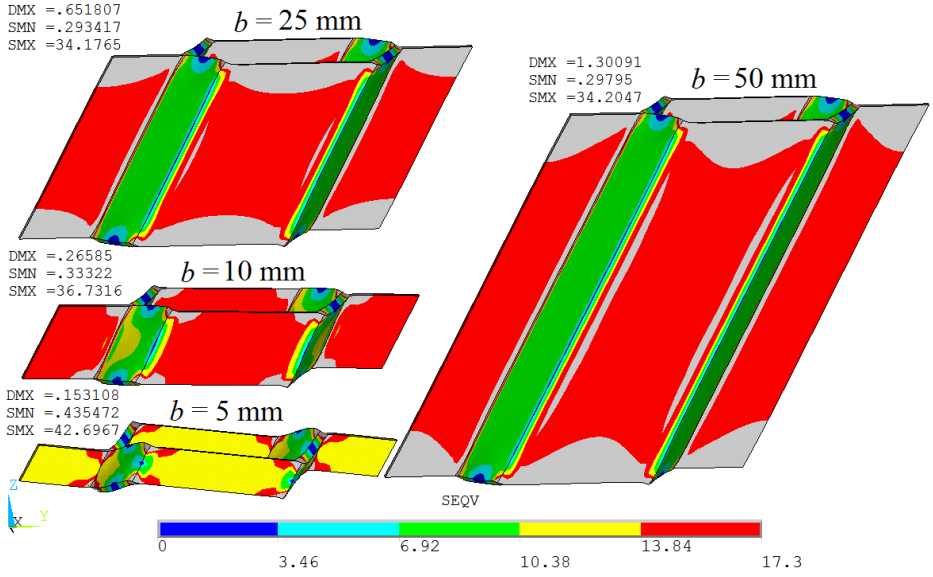

Fig. 13 – Von Mises stress distribution [MPa] for four different cell heights obtained from load case 5, corresponding to G_{23} computation at an imposed shear strain $\bar{\gamma}_0$ =0.026 rad. Scaling of displacement 20X

7. CONCLUSIONS

The results of numerical investigations confirm the validity of all models proposed in this paper for the computation of mechanical properties of honeycombs. These models can be used for parametric or sensitivity analyses as they were presented in two paragraphs. The proposed models can be also used with minor corrections for the analysis of real commercial honeycombs including the curved and perforated cell walls.

The analytical relation (15) was corrected by the authors of this paper and then confirmed using FEAs, as it wasn't adequately presented in [1].

The developed APDL codes for the proposed models can be effortless adapted to new honeycomb types as those proposed in [9, 25, 26], and can include special composite materials by considering the wall thickness or can include the thickness of the adhesive layer in the finite element model.

Further on, the reduction of RVE to the base unit cell member or even to a half of it, depending on the symmetry or anti-symmetry of the load cases, as in [5, 8, 16], especially for the 3D solid model, will get the authors' attention in order to reduce the computational effort.

ACKNOWLEDGEMENT

This work was supported by a grant of the Romanian National Authority for Scientific Research, CNDI–UEFISCDI, project number PN-II-PT-PCCA-2011-3.2-0068, contract 206/2012.

REFERENCES

[1] L. J. Gibson and M. F. Ashby, *Cellular Solids, Structure and properties*, Cambridge University Press, Cambridge, 1997.

[2] A. Imran and J. J Yu, Mathematical Models for in-Plane Moduli of Honeycomb Structures-A Review, *Research Journal of Applied Sciences, Engineering and Technology*, vol. **7**, no. 3, pp. 581-592, 2014.

[3] Y. M. Li, M. P. Hoang, B. Abbes, F. Abbes, Y.Q. Guo, Analytical homogenization for stretch and bending of honeycomb sandwich plates with skin and height effects, *Compos. Struct.*, vol. **120**, pp 406–416, 2015.

[4] A. Spadoni, *Application of Chiral Cellular Materials for The Design of Innovative Components*, PhD Thesis, Georgia Institute of Technology, December 2008.

[5] A. Alderson, K. L. Alderson, D. Attard, K. E. Evans, R. Gatt, J. N. Grima, W. Miller, N. Ravirala, C. W. Smith, K. Zied, Elastic constants of 3-, 4- and 6-connected chiral and anti-chiral honeycombs subject to uniaxial in-plane loading, *Composites Science and Technology*, Vol. **70**, no. 7, pp. 1042-1048, 2010.

[6] S. Balawi, J. L. Abot, The effect of honeycomb relative density on its effective in-plane elastic moduli: An experimental study, *Compos. Struct.*, vol. **84**, pp. 293–299, 2008.

[7] J. Dirrenberger, S. Forest, D. Jeulin, C. Colin, Homogenization of periodic auxetic materials, *Procedia Engineering*, vol. **10**, pp. 1847–1852, 2011.

[8] C. Lira, P. Innocenti, F. Scarpa, Transverse elastic shear of auxetic multi re-entrant honeycombs, *Compos. Struct.*, vol. **90**, pp. 314–322, 2009.

[9] W. Miller, C.W. Smith, K.E. Evans, Honeycomb cores with enhanced buckling strength, *Compos. Struct.*, vol. **93**, pp. 1072–1077, 2011.

[10] T. C. Lin, M. Y. Yang, J. S. Huang, Effects of solid distribution on the out-of-plane elastic properties of hexagonal honeycombs, *Compos. Struct.*, vol. **100**, pp. 436–442, 2013.

[11] J. Ju, J.D. Summers, Compliant hexagonal periodic lattice structures having both high shear strength and high shear strain, *Materials and Design*, vol. **32**, pp. 512–524, 2011.

[12] J. N. Grima, R. Cauchi, R. Gatt, D. Attard, Honeycomb composites with auxetic out-of-plane characteristics, *Compos. Struct.*, vol. **106**, pp. 150–159, 2013.

[13] A. Karakoç, K. Santaoja, J. Freund, Simulation experiments on the effective in-plane compliance of the honeycomb materials, *Compos. Struct.*, vol. **96**, pp. 312–320, 2013.

[14] J. P. M. Whitty, F. Nazare, and A. Alderson, *Modelling the effects of density variations on the in-plane Poisson's ratios and Young's Moduli of periodic conventional and re-entrant honeycombs - Part 1: Rib thickness variations*, 2002, IMRI: Journal Articles, http://digitalcommons.bolton.ac.uk/cmri_journalspr/2.

[15] A. Vigliotti, D. Pasini, Linear multiscale analysis and finite element validation of stretching and bending dominated lattice materials, *Mechanics of Materials*, vol. **46**, pp. 57–68, 2012.

[16] V. N. Burlayenko, T. Sadowski, Effective elastic properties of foam-filled honeycomb cores of sandwich panels, *Compos. Struct.*, vol. **92**, pp. 2890–2900, 2010.

[17] S. Balawi, J. L. Abot, A refined model for the effective in-plane elastic moduli of hexagonal honeycombs, *Compos. Struct.*, vol. **84**, pp 147–158, 2008.

[18] I. G. Masters, and K. E. Evans, Models for the elastic deformation of honeycombs, *Compos. Struct.*, vol. **35**, no. 4, pp. 403-422, 1996.

[19] Y. J. Chen, F. Scarpa, Y. J. Liu, J. S. Leng, Elasticity of anti-tetrachiral anisotropic lattices, *International Journal of Solids and Structures*, vol. **50**, no. 6, pp. 996-1004, 2013.

[20] M. Grediac, A finite element study of the transverse shear in honeycomb cores, *International Journal of Solids and Structures*, vol. **30**, no. 13, pp. 1777-1778, 1993.

[21] S. Kelsey, R. A. Gellatly and B. W. Clark, The shear modulus of foil honeycomb cores, *Aircraft Engineering*, pp. 294-302, 1958.

[22] Y. Prawoto, Seeing auxetic materials from the mechanics point of view: A structural review on the negative Poisson's ratio, *Computational Materials Science*, vol. **58**, pp 140–153, 2012.

[23] A. Sharma, B. V. Sankar, R. T. Haftka, *Homogenization of Plates with Microstructure and Application to Corrugated Core Sandwich Panels*, AIAA Paper 2010-2706.

[24] D. H. Chen, S. Ozaki, Analysis of in-plane elastic modulus for a hexagonal honeycomb core: Effect of core height and proposed analytical method, *Compos. Struct.*, vol. **88**, pp. 17–25, 2009.

[25] A. Bezazi, F. Scarpa, C. Remillat, A novel centresymmetric honeycomb composite structure, *Compos. Struct.*, vol. **71**, pp. 356–364, 2005.

[26] A. Bezazi, C. Remillat, P. Innocenti, F. Scarpa, In-plane mechanical and thermal conductivity properties of a rectangular–hexagonal honeycomb structure, *Compos. Struct.*, vol. **84**, pp. 248–255, 2008.

[27] *** ANSYS, *Theory Reference*. ANSYS Academic Research, Release 15.0, 2014.